Evolution of far-from-equilibrium nanostructures on Ag(100) surfaces: Protrusions and indentations at extended step edges

A. M. Cadilhe, C. R. Stoldt, C. J. Jenks, P. A. Thiel, and J. W. Evans
IPRT, Departments of Chemistry and Mathematics, and Ames Laboratory, Iowa State University, Ames Iowa 50011
(Received 4 June 1999)

Scanning tunneling microscopy is used to monitor the formation and relaxation of nanoprotrusions and nanoindentations at extended step edges following submonolayer deposition of Ag on Ag(100). Deposition of up to about 1/4 ML Ag produces isolated two-dimensional (2D) Ag clusters, which subsequently diffuse, collide, and coalesce with extended step edges, thus forming protrusions. Deposition of larger submonolayer amounts of Ag causes existing step edges to advance across terraces, incorporating 2D islands. The resulting irregular step structure rapidly straightens after terminating deposition, except for a few larger indentations. Relaxation of these far-from-equilibrium step-edge nanoconfigurations is monitored to determine rates for restructuring versus local geometry and feature size. This behavior is analyzed utilizing kinetic Monte Carlo simulations of an atomistic lattice-gas model for relaxation of step-edge nanostructures. In this model, mass transport is mediated by diffusion along the step edge (i.e., ''periphery diffusion''). The model consistently fits observed behavior, and allows a detailed characterization of the relaxation process, including assessment of key activation energies.

I. INTRODUCTION

The response of physical systems to *slight* perturbations from equilibrium, or even to spontaneous fluctuations about the equilibrium state, determines macroscopic transport coefficients.[1] However, in general, one would expect that the relaxation of systems *far* from equilibrium can provide more detailed information into underlying transport processes. Indeed, various stages of such relaxation might be controlled by distinct microscopic processes, so activation barriers specific to these could potentially be extracted from the kinetics. In this paper, we present a detailed characterization of the relaxation of far-from-equilibrium two-dimensional (2D) step-edge nanostructures on Ag(100) surfaces at room temperature to gain fundamental insight into the atomic-scale processes mediating the approach to equilibrium or relaxation. This theme fits with a number of other recent studies of relaxation processes for both submonolayer[2–5] and multilayer[6–9] metal films, shifting somewhat from the primary focus of the last decade on the formation of nonequilibrium structures during deposition.[10]

The viability of such studies requires, of course, that the relaxation dynamics occurs on experimentally accessible time scales. Somewhat surprisingly, for metal surfaces near room temperature, this feature has been demonstrated by a number of scanning tunneling microscopy (STM) studies. These reveal that rather than being ''static,'' metal surfaces can actually be in a state of flux. This is evidenced by the equilibrium fluctuations or ''frizziness'' of monoatomic step edges on Cu, Au, and Ag surfaces.[11] In addition, evolution of nonequilibrium submonolayer or multilayer structures created either by deposition,[10] or mechanically using the STM tip,[12,13] has been observed.

Next, we briefly review previous studies of dynamics and relaxation at step edges, which are most relevant to this study. First, we emphasize that most previous STM investigations have focussed on the near-equilibrium dynamics of monoatomic step edges. Above mentioned studies of ''frizziness,''[11] and similar studies of step-edge roughness,[14,15] have elucidated both mass transport and energetics at step edges. In similar studies, the time-correlation functions describing equilibrium fluctuations of step edges have been analyzed in order to assess such mass transport processes and effective transport coefficients.[16] More recently, there have been reports of a few studies of the relaxation of more exotic far-from-equilibrium step-edge nanostructures, precisely the focus of the current study. Our group has characterized the relaxation of protrusions at step edges on Ag/Ag(100) surfaces,[17,18] and the restructuring of pairs of near-square adatom clusters for both side-on or corner-to-corner collisions.[17–20] Analogous observations have been reported for the decay of protrusions at step edges on Cu/Cu(111) surfaces,[21] and for corner-to-corner cluster collisions on Cu/Cu(100) surfaces.[22] Relaxation subsequent to collision of vacancy clusters with other clusters and with step edges has been analyzed for Ag/Ag(111) surfaces.[23] Finally, we mention that the analogous coalescence or sintering of pairs of 3D clusters has been observed long ago,[24] and there have been some recent theoretical developments on this topic.[25]

A general understanding of these processes comes from the recognition that relaxation is driven by reduction in the free energy of the step edge, and noting that this free energy is typically dependent on step orientation.[16,26] For larger structures or larger characteristic lengths, it is reasonable to adopt a coarse grained or continuum description of step-edge structure. Then fluctuation or relaxation dynamics are described by a continuum evolution equation, which assumes a Langevin form when incorporating noise to describe fluctuation dynamics.[26] Indeed this approach has been successfully applied to analyze both near-equilibrium fluctuations,[16,26] and relaxation of far-from-equilibrium structures.[21,23] These equations involve effective transport coefficients, which can

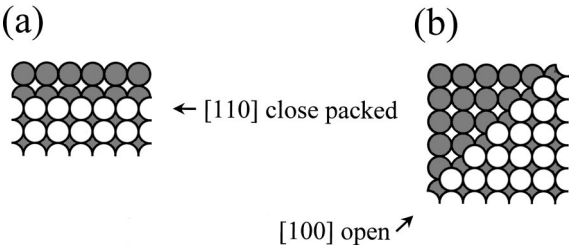

FIG. 1. Schematic of the structure of: (a) a close-packed [110] step edge; (b) an open [100] step edge, on an fcc(100) metal surface.

be determined by fitting to experimental data. Despite some success with continuum modeling, there are a number of reasons why a more detailed atomistic description is preferred or even necessary in our studies of relaxation processes. First, a range of quite small structure sizes is probed in the experiments, so one should question the applicability of the continuum approach. Second, we are interested in assessing activation barriers for specific microscopic processes controlling relaxation, which constitute the input of atomistic models. Third, we also wish to compare relaxation dynamics introducing a variety of competing microscopic processes and pathways into our atomistic models. Fourth, fluctuations can be significant in the decay of smaller structures, and atomistic simulations provide direct information on this behavior. Thus, we shall focus on the analysis of experimental data with an atomistic model, making only some brief comments on corresponding behavior predicted by continuum descriptions.

This paper will present a detailed analysis of the relaxation of both far-from-equilibrium nanoprotrusions and nanoindentations at extended step edges on Ag(100) surfaces at room temperature. The nanoprotrusions are typically formed according to the following scenario. Deposition of up to $\sim$0.25 ML of Ag produces isolated 2D Ag clusters, with near-square shapes having close-packed [110] step edges [Fig. 1(a)]. These subsequently diffuse intact,[4,27] collide, and coalese with extended step edges.[18] The predominant, equilibrium step-edge orientation is [110], and clusters collide side on with such step edges creating an initial square protrusion. However, for various reasons enumerated below, our surfaces also present some ''metastable'' open [100] step edges [Fig. 1(b)], oriented at 45° to [110] step edges. Clusters collide corner on with these steps, creating a ''nodule,'' which relaxes through an intermediate triangular shape.[18] Nanoindentations are typically formed after deposition of larger submonolayer amounts of Ag. This leads to significant advance of existing step edges across terraces, and incorporation of 2D Ag clusters ahead of the step edge. The result is a highly irregular step-edge structure, which restructures rapidly after terminating deposition, often leaving locally straight steps with various orientations having a few larger nanoindentations. STM observations of these relaxation processes are analyzed with an appropriate atomistic lattice-gas model for mass transport via periphery diffusion.[18] In particular, we explore the dependence of the relaxation dynamics on feature size and step orientation.

In Sec. II, we briefly describe the experimental setup and procedure for preparation of the desired initial surface morphology (i.e., step-edge nanostructures). In Sec. III, we describe in some detail our atomistic lattice-gas model for restructuring where mass transport is mediated by periphery diffusion of adatoms along the step edge. We also mention alternative mass transport mechanisms, together with some indications from previous studies that periphery diffusion (rather than the other mechanisms) should dominate restructuring. In Sec. IV, we examine specifically the relaxation of nanoprotrusions at both [110] and [100] step edges. Some analysis of observed behavior is provided, as well as a comparison of behavior for the different step orientations. A briefer but analogous discussion of relaxation of nanoindentations is provided in Sec. V. Extending the investigation in Sec. IV, we note in Sec. VI that other unusual step edge nanoprotrusions can be fabricated with the STM tip. Specifically, we discuss the formation and relaxation of elongated rectangular protrusions orthogonal to [110] step edges. A brief discussion of the predictions of simplified continuum theories is provided in Sec. VII, and of interaction energetics and modified lattice-gas models for periphery diffusion is provided in Sec. VIII. Finally, some conclusions are presented in Sec. IX.

II. EXPERIMENTAL SETUP AND PREPARATION OF SURFACE MORPHOLOGIES

The key details of the experimental setup[3,17,18] are first described briefly. We use an Omicron room-temperature STM housed in an ultrahigh vacuum chamber with base pressure of below 10^{-10} Torr. The Ag(100) substrate is prepared through cycles of Ar-ion sputtering and annealing to 700 K. Contamination is minimal based on inspection of STM images, and on Auger spectroscopy analysis. Initial film configurations were created by evaporative deposition of Ag from a home-built liquid nitrogen shrouded source onto an Ag(100) single-crystal surface always held at room temperature (298 ± 3) K. Large area scans of post-deposition evolution were taken at intervals of 3–15 min. Rates of change of key dimensions were then monitored, these dimensions being obtained consistently using the full width at half maximum of the scan profiles. The database presented here was obtained on a variety of single crystals, and with various tunneling conditions (although these were generally chosen to minimize tip-surface interactions, e.g., voltage $=0.7-1.5$ V, current$=0.3-0.5$ nA). The selfconsistency of the database indicates that STM-tip effects do not significantly influence nanostructure evolution.

Before focusing on the evolution of nanostructures in subsequent sections, it is appropriate to give a broader view of the type of morphologies created by the above deposition experiments. Three qualitatively distinct possible morphologies observed immediately after deposition are illustrated in Fig. 2, each of which is directly relevant to the current study. In Fig. 2(a), we show a highly stepped portion of the crystal surface where the extended monoatomic steps display nearly parallel alignment in the equilibrium [110] direction. Deposition leads to island formation only on the broader terraces between steps, as all deposited atoms on narrower terraces are captured by the step edges. Diffusion of these islands[27] can lead to side-on collision with ascending step edges forming near-square protrusions which subsequently relax. In Fig. 2(b), we show a broad terrace bordered by monoatomic step

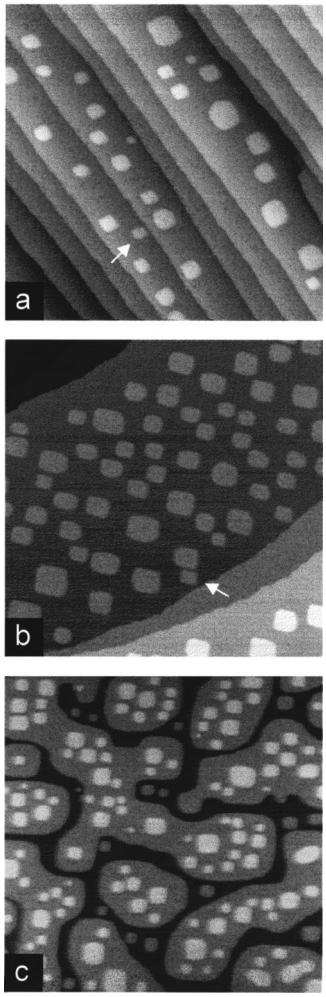

FIG. 2. (a) $2180\times2180\,\text{Å}^2$ region of the surface with a dense array of parallel [110] steps, subsequent to deposition and formation of 2D Ag islands. The island indicated by the arrow collides with the ascending step edge. (b) $1580\times1580\,\text{Å}^2$ region of the surface with a broad terrace bordered by bent step edges, subsequent to deposition of 0.29 ML of Ag. One of the 2D islands thus formed (indicated by an arrow) collides with a portion of the step edge with local [100] orientation. (c) $2000\times2000\,\text{Å}^2$ region of the surface subsequent to deposition of 0.8 ML Ag, extended annealing at 298 K, and then further deposition of 0.6 ML of Ag.

edges which are ''bent'' from the [110] orientation, presumably due to pinning by impurities or some defect outside the field of view. In some regions the step has roughly a [100] orientation, so nearby islands formed after deposition naturally collide corner on to this portion of the step. Finally, in Fig. 2(c), we show a more complicated morphology. This was created by first depositing about 0.8 ML of Ag, and then allowing extended annealing at room temperature, which leads to the formation of large ramified filled regions with various metastable step orientations.[3] Subsequently, an additional 0.6 ML of Ag was deposited to form smaller islands in both the first and second layer. Diffusion of the first layer islands leads to collision with step edges having various orientations. Examples from these different types of experiments are utilized to assess the relaxation and decay of nanoprotrusions.

In Sec. I, we mentioned that extended deposition of around 0.6–0.8 ML of Ag can lead to the formation of isolated indentations in extended step edges. More detailed discussion and examples of such process are presented in Sec. V where we discuss the decay of nanoindentations.

III. ATOMISTIC MODELS FOR MASS TRANSPORT AT STEP EDGES

We first briefly discuss possible mechanisms or pathways for mass transport on surfaces,[16,26,27,28] which could control relaxation of step-edge nanostructures. A natural candidate is *periphery diffusion* (PD), wherein atoms hop along the step edge, but do not detach from it, or attach to it (e.g., from some dilute 2D gas phase). Another reasonable possibility is *terrace diffusion* (TD). The most commonly considered case involves the correlated detachment, diffusion, and reattachment of *adatoms* at the step edge (TDA), where the latter process is not inhibited by an extra barrier relative to terrace diffusion. There is an analogous process involving the formation/detachment, and diffusion of *vacancies* into the step edge, and their subsequent reattachment (TDV). Finally, we mention *evaporation-condensation* (EC), involving the uncorrelated detachment and attachment of adatoms (or vacancies) at the step edge, a scenario that is usually associated with an additional barrier to attachment. The latter is regarded as unlikely for metal homoepitaxial systems. As indicated in Sec I, we believe that periphery diffusion provides the dominant relaxation mechanism for the Ag(100) system at room temperature. Thus, below, we first describe in detail the atomistic PD model used to analyze experimental data. Finally, we comment briefly on the other mechanisms, indicating previous experimental observations and some theoretical arguments supporting our claim that they should not be dominant in the regime of interest for our system.

A. Periphery diffusion mechanism

Atomistic lattice-gas models for mass transport at step edges mediated by *periphery diffusion* (PD) have already been applied to analyze the following processes: cluster diffusion;[29,30] diffusion-mediated growth of islands during deposition, and associated shape instabilities;[31] the post-deposition equilibration of island shapes;[32,18] and relaxation at step edges (in our preliminary work).[18] In these PD models, it is important to distinguish between a number of key hopping processes at the atomic level. The most important of these include: fast *e*dge diffusion along straight close-packed [110] steps at rate h_e; *k*ink escape at rate h_k; corner *r*ounding at rate h_r; and slow ''*c*ore breakup'' at rate h_c. See Fig. 3. As an aside, we note that the ''corner rounding'' process is crucial for island shape stability during growth.[31] Also, the term ''core breakup'' is borrowed from our previous work on diffusion of large clusters, where this process is shown to be necessary for long-range movement of the entire cluster.[27,29] All these rates will be assumed to have an Arrhenius form

$$h_i = \nu_i \exp[-E_i/(k_B T)], \tag{1}$$

where $i=e,\ k,\ r,$ or c indicates the hopping process.

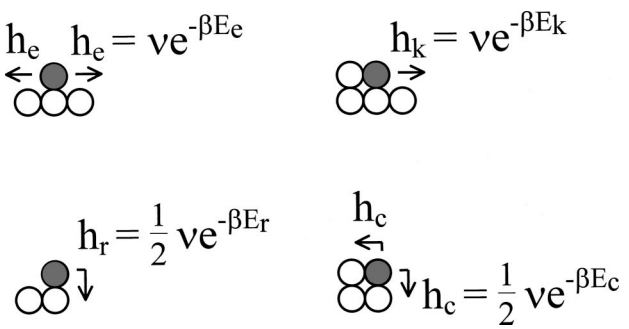

FIG. 3. Schematic showing the four atomic hopping processes (for the shaded atom) included in our PD model: edge diffusion at rate h_e (top left), kink escape at rate h_k (top right), corner rounding at rate h_r (bottom left), and core breakup at rate h_c (bottom right).

Note that in the schematic Fig. 3, and in our modeling, the two distinct hops or steps involved in both corner rounding and core breakup are treated as a single step. For these cases, after the first ''difficult'' hop where the atom reaches a site diagonally adjacent to the closest atom in the step edge, there is a roughly equal chance for it to return to its original site, rather than to continue to complete the process. Thus, treating these two hops as a single step, we somewhat arbitrarily assign reduced prefactors $\nu_r = \nu_c = \nu/2$ for these two-hop processes, compared with $\nu_e = \nu_k = \nu$ for the other two processes. We also set $\nu = 10^{12}\,\mathrm{s}^{-1}$. The factor of 1/2 in ν_r and ν_c reflects the 50% ''success rate'' for these processes after the first hop, and thus corresponds to choosing a single prefactor ν for all single hops. Treating corner rounding and core breakup as a single-step simplifies the modeling by restricting allowed configurations to those having nearest-neighbor (NN) connectivity.

Next, we discuss in some detail the choice of activation barriers E_i as these primarily control the magnitude of the hopping rates. Thus, a physically realistic choice of these energies is essential to correctly describe the kinetics of mass transport at step edges. We model the Ag/Ag(100) system assuming that the energies of various configurations of adatoms *located at the adsorption sites* can be described with *effective* NN pairwise adatom interactions of magnitude J. Thus, atoms on NN sites separated by the surface lattice constant, a, have interaction J, but those on diagonal or next-NN sites separated by $\sqrt{2}a$ have negligible interaction.[18] Then, some basic relationships between the above rates or barriers can be obtained noting that kink escape and edge diffusion correspond to forward and reverse processes between configurations whose energies differ by J. The same applies for core breakup and corner rounding. Thus, the detailed-balance relationship between rates for forward and reverse processes[18,32–34] implies that

$$h_k/h_e = h_c/h_r = \exp[-J/(k_B T)]. \tag{2}$$

As discussed further below, semiempirical calculations for metal(100) homoepitaxy[29,33,34] suggest that $h_r \approx h_k$, so we choose

$$E_r \approx E_k = E_e + J, \text{and thus } E_c \approx E_e + 2J. \tag{3}$$

Another reasonable expectation for metal(100) homoepitaxy is that $E_e \approx E_d/2$, where E_d is the activation barrier for hopping of adatoms across terraces (see below, and Sec. III B). Thus, for the Ag/Ag(100) system where[19,35,36] $E_d \approx 0.40\,\mathrm{eV}$, this relationship implies that $E_e \approx 0.20\,\mathrm{eV}$. This leaves one free parameter J in our model. This parameter will be adjusted to match experimental behavior for the decay protrusions at [110] step edges, and then we will assess the success of the model in predicting decay for other nanoconfigurations.

Some further discussion of the above choices for activation barriers is appropriate. Pioneering studies of the barriers for hopping in the Ag/Ag(100) system by Voter,[29] using semiempirical embedded atom method (EAM) potentials, indicated that both $E_r \approx E_k$ and $E_e \approx E_d/2$ (in part motivating our choice). The latter choice is also supported by *ab initio* local-density approximation (LDA) studies,[37] which predict that $E_e/E_d \approx 0.56$. The general ordering that $E_r \approx E_k$, and that E_e is far smaller than E_d, is also supported by semiempirical studies for Ag/Ag(100) [Ref. 33] and Cu/Cu(100) (Refs. 34 and 38), which suggest that activation barriers for all local configurations of the hopping particle fall into a few distinct classes.

This behavior, and the above choices, are quite distinct from the ''traditional'' choice,[39] for activation barriers with NN interactions J, of $E_i = E_d + n_i J$, where n_i is the number of nearest neighbors in the *initial* state. Further, we note that various other distinct choice of barriers are consistent with detailed balance (e.g., $h_r \approx h_e$ and $h_c \approx h_k$). These choices would no doubt exhibit quite different relaxation kinetics. At first glance, the dramatic difference between our choice and the traditional one might be taken to imply the existence of strong next-NN interactions (which would be inconsistent with the stated assumptions). However, this is not the case. The form we have chosen (which is based on the behavior of semiempirical interactions) reflects the presence of strong interactions (comparable to J) in the *transition state*[34] for each of the hopping processes $i = e,k,r,c$. This feature presumably reflects the fact that the distance of the hopping atom to the closest step edge atoms in the transition state ($\sqrt{5}a/2 \approx 1.12a$) is significantly less than the distance between next-NN sites ($\sqrt{2}a \approx 1.41a$). [Note that these distance estimates neglect relaxation of atom positions.] The same feature is seen to some extent modeling adatom interactions with pairwise Lennard-Jones potentials.[40] This strong interaction in the transition state explains why the traditional choice is completely inadequate.

In this paper we implement the simplest possible PD model incorporating only the above four processes.[18] This means that the system evolves through configurations satisfying NN connectivity. No atoms with three or more occupied neighbors are mobile, and no internal vacancies are created. Strictly speaking, this model violates detailed balance since, e.g., an atom can reach a triply coordinated site by corner rounding, but the reverse process is forbidden. However, we argue that such events are rare, and so will not significantly influence the far-from-equilibrium decay processes of interest here (in contrast to behavior near equilibrium). Further discussion of these issues, and possible model refinements including modified choices for activation barriers, is provided in subsequent sections (particularly Sec. VI describing decay of nanoindentations, and also Sec. VIII).

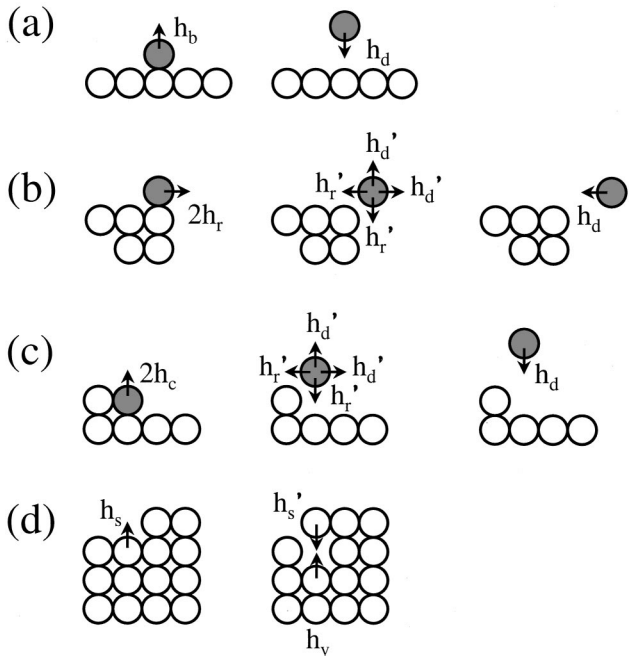

FIG. 4. Schematics for TDA (a)–(c) and TDV (d). Descriptions below correspond to frames from left to right. (a) Atom detachment from a straight [110] step edge at rate h_b, and attachment at rate h_d. (b) The first step of corner rounding (at rate $2h_r$); return or continued corner rounding at rate h_r', or detachment at rate h_d' (from the site diagonally adjacent to the corner of the step edge); ''attachment'' to the site diagonally adjacent to the corner at rate h_d. (c) Atom detachment from a kink site (at rate $2h_c$); return or corner rounding at rate h_r', or detachment at rate h_d' (from the site diagonally adjacent to the kink); ''attachment'' to the site diagonally adjacent to the kink at rate h_d. (d) Vacancy detachment from a kink site (with ''sliding'' rate h_s; see Sec. V B); reattachment at rate h_s', or further detachment at rate h_v.

A key goal of this paper is to assess the effective activation barrier $E_{\rm act}$ for the decay of protrusions and indentations at extended step edges. For relaxation mediated by *periphery diffusion*, we show in detail in Secs. IV and V that the effective barrier for the overall decay process is equal to that for the slowest atomistic step of core breakup, so[18]

$$E_{\rm act}({\rm PD}) \approx E_e + 2J = E_c . \tag{4}$$

B. Other mass transport mechanisms

We consider first *terrace diffusion of adatoms* (TDA), which involves detachment or evaporation from the step edge, diffusion across the terrace with hop rate h_d, and reattachment to the step edge (also at rate h_d). Below, we set $h_d = \nu_d \exp[-E_d/(k_B T)]$, with $\nu_d = \nu = 10^{12}\,{\rm s}^{-1}$. Note that adatoms can detach from various local environments, e.g., from a straight [110] step edge [Fig. 4(a)], while rounding a corner [Fig. 4(b)], or from a kink site [Fig. 4(c)]. We now show that these all occur with the same overall effective rate. Again, we restrict our attention to the case of effective NN interactions J and choose activation barriers for attachment and detachment rates [shown in Figs. 4(a)-4(c)] in a way consistent with Sec. III A. Thus, attachment rates from the most distant site are set to h_d. Detailed balance then also implies that

$$h_b = \exp[-J/(k_B T)] h_d , \quad h_d' = h_d , \quad \text{and}$$
$$h_r' = 1/2 \exp[J/(k_B T)] h_r = 1/2 \exp[2J/(k_B T)] h_c = 1/2 h_e . \tag{5}$$

[Note that the above results also show that $h_d' \ll h_r'$, since $h_d \ll h_e$ (see below), which explains why detachment is unlikely during corner rounding, a necessary condition for the occurrence of PD.] It is important to emphasize that the effective rate of detachment, $h_{\rm detach}$, is *not* determined solely by the rate for the slowest individual step during detachment. Instead, one assumes a quasiequilibrium for configurations before this last step, and notes that the probability of the initial configuration in Figs. 4(a)-4(b) corresponds to the (low) density, $\rho_{eq} \sim h_k/h_e \sim \exp[-J/(k_B T)]$, of isolated edge atoms. Then, identifying h_{detach} as the rate for the last detachment step times the probability of the configuration before that hop, one obtains[18,41]

$$h_{\rm detach} \sim \rho_{eq} h_b \ \text{ in Fig. 4(a)}, \ \rho_{eq}(h_r/h_r')h_d' \ \text{ in Fig. 4(b)},$$
$$\text{and } 1 \cdot (h_c/h_r')h_d' \ \text{ in Fig. 4(c)}. \tag{6}$$

Thus, in all cases, one finds that

$$h_{detach} \sim \nu \exp[-2J/(k_B T)] h_d ,$$

and consequently that

$$E_{\rm act}({\rm TDA}) = E_d + 2J. \tag{7}$$

This result is consistent with the idea that mass transport is limited by terrace diffusion for TD processes. To see this, recall the exact Onsager form[42] for the equilibrium density of the dilute 2D gas phase, $\rho_{\rm gas} \sim \exp[-2J/(k_B T)]$, which coexists with the 2D condensed phase (i.e., large islands or steps). Mass transport is determined by the rate of attachment, $h_{\rm attach} \sim \rho_{\rm gas} h_d$, of atoms in this 2D gas phase to each perimeter site of the condensed phase. Using Onsager's result, it is clear that $h_{\rm attach}$ corresponds to $h_{\rm detach}$, thus recovering Eq. (7).

Comparing Eqs. (4) and (7), it follows that for Ag/Ag(100) where we set $E_d \approx 0.40$ eV and $E_e \approx 0.20$ eV, there is an *energetic advantage* equal to $E_d - E_e \approx 0.2$ eV for PD over TDA. Thus PD should dominate TDA, at least for small-size features, and certainly for lower temperatures. It is however quite possible that a crossover occurs for larger feature sizes where other mechanisms may have a ''statistical advantage'' over PD. This type of crossover is also expected for cluster diffusion in metal(100) homoepitaxial systems, where simplistic arguments indicate a slower decrease of diffusivity with cluster size for TDA than for PD.[27,30] This slower decrease should eventually overcome the energetic disadvantage of the former. Continuum Langevin-type equation treatments of cluster diffusion also support the existence of a crossover.[26]

Next, we consider *terrace-diffusion of vacancies* (TDV). We suppose that the hop rate for isolated vacancies has the form $h_v = \nu_v \exp[-E_v/(k_B T)]$, with $\nu_v = \nu = 10^{12}\,{\rm s}^{-1}$. As for TDA, one can show that the effective rate, $h_{\rm detach}$, for vacancy detachment is independent of the local step configuration. Considering detachment from kinks shown in Fig. 4(d), detailed-balance implies $h_s/h_s' = \exp[-2J/(k_B T)]$ (see also

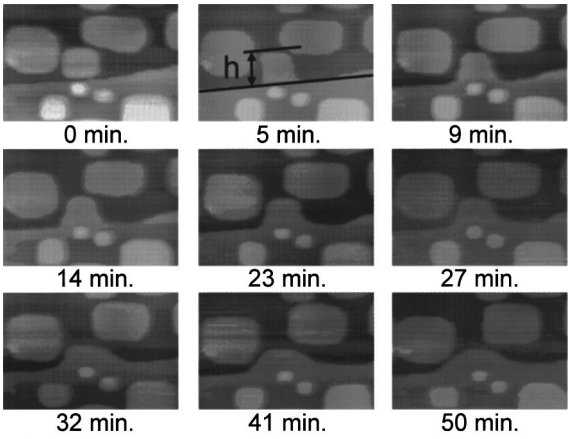

FIG. 5. Sequence of STM images showing coalescence of a 105×130 Å^2 cluster with a [110] step edge, and subsequent decay of the protrusion thus formed. All images are 400×600 Å^2. Determination of $h_\square$ is indicated in the second frame.

Sec V B), and it follows that $h_{\rm detach}=(h_s/h_s')h_v$. Mass transport is also determined by the rate of vacancy attachment, $h_{\rm attach}\sim\rho_{\rm gas}h_v$. From either result, one obtains

$$E_{\rm act}({\rm TDV})=E_v+2J. \tag{8}$$

Based on simulation studies choosing $E_v=E_e$,[43] it was recently suggested that TDV rather than PD mediates mass transport in the observed diffusion of large 2D clusters in metal(100) homoepitaxial systems. However, the significance of TDV (relative to PD) clearly depends on the value of E_v (relative to E_e). Semiempirical studies for the Ag/Ag(100) system suggest that[29,44] $E_v/E_e\approx1.8$ (and $E_v/E_d\approx1$) implying a significant *energetic advantage* for PD over TDV.[45,46] This contrasts the simulation studies in Ref. 43, where there is no energetic advantage.

For *evaporation-condensation* (EC) with an additional barrier to attachment δE one has that $E_{\rm act}({\rm EC})=E_{\rm act}({\rm TD})+\delta E$, reflecting an even greater energetic disadvantage relative to PD. Another possibility for EC is that uncorrelated attachment-detachment may occur without an additional barrier when many islands or protrusions are close to each other as a result of mass flow between them. In this case, the activation barrier would correspond to that for TD.

IV. DECAY OF PROTRUSIONS AT EXTENDED STEP EDGES

We now discuss in detail our experimental observations for the coalescence or ''sintering'' of 2D clusters with step edges, and the subsequent decay of protrusions thus formed. Behavior is analyzed using simulations of our PD model. Below, rates for relaxation (i.e., growth or decay of key linear dimensions) are quoted in terms of the surface lattice constant, $a=2.89$ Å for Ag(100).

A. Cluster+[110] step coalescence

After side-on collision of a diffusing cluster with a [110] step edge, and ''initial'' far-from-equilibrium configuration is created consisting of a square protrusion at this straight step edge. This protrusion decays smoothly, leading to eventual recovery of a straight step edge. A sequence of STM images for such a process is shown in Fig. 5. The key quantity of interest is the maximum height of the protrusion $h_\square$ measured relative to the mean position of the step edge, as indicated in Fig. 5. The decay of $h_\square$ is observed to be roughly linear in time, for the earlier part of the decay process (see Fig. 6). In contrast, the area A of the protrusion is roughly constant (noting that, for later stages of decay, it is difficult to delineate the protrusion from the step edge, and thus to determine A). Analysis of such experimental data for protrusions of various sizes or areas indicates a roughly linear variation of this initial decay rate $R_\square=dh_\square/dt$ (for earlier times), with the inverse area of the protrusion A^{-1}. This data is summarized in Fig. 7.

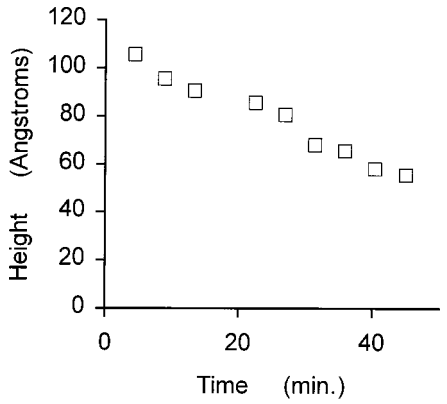

FIG. 6. Decay of height of the protrusion shown in the sequence of STM images in Fig. 5.

This relaxation process is modeled via kinetic Monte Carlo simulations using our atomistic PD model, and starting with a perfect square protrusion attached to a perfectly straight [110] step edge. A typical sequence of configurations for a decaying square protrusion with an initial size of 30 $\times30$ atoms at 298 K and with $J=0.275$ eV, is shown in Fig. 8. The decrease with time of the height of the protrusion, $h_\square$, is shown in Fig. 9, together with behavior for a range of other initial sizes (using the same T and J). This value of $J=0.275$ eV for the effective NN interaction (together with the previously assigned choices $E_e=0.20$ eV, and ν

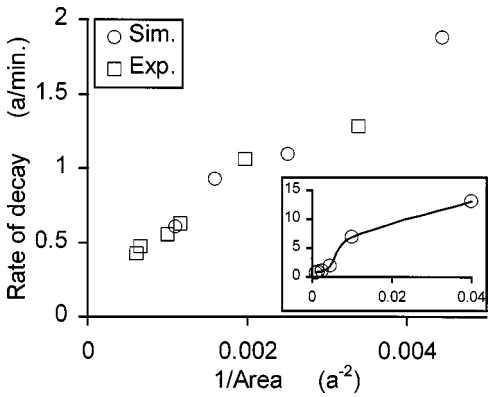

FIG. 7. Initial rate of decay of the height of square protrusions at a [110] step edge versus 1/Area: ''squares'' represent experimental data, and ''circles'' represent PD model predictions with $J=0.275$ eV. The inset shows nonlinear variation of rate with 1/Area in the PD model for a range of smaller protrusion sizes.

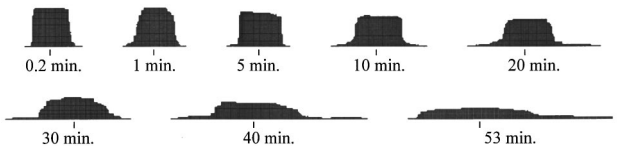

FIG. 8. Simulated sequence of configurations for an initially 30×30 atom protrusion decaying on a [110] step edge (of length $1000a$) for up to 53 min of physical time, or a 70% decay of the initial height. The portion of the step edge shown is $46a$ at 0.2 min, $51a$ at 1 min, and 5 min, $76a$ at 10 min, $106a$ at 20 min, $101a$ at 30 min, $156a$ at 40 min, and $157a$ at 53 min.

$=10^{12}$ s) is chosen so that PD model values for $R_{\square}$ taken from Fig. 9 match the experimental observations. The simulation results are plotted together with the experimental data in Fig. 7. The inset to Fig. 7 also shows the simulation predictions for decay rates $R_{\square}$ for a range of much smaller protrusion sizes than observed in experiment. A strong nonlinear variation of rate with inverse area is apparent over this broader size range.

Our simulations also confirm the equality $E_{\rm act}({\rm PD})\approx E_e+2J=E_c$ (cf. Sec. III) for the effective activation barrier for the overall decay process. See Sec. IV (C) for further discussion. Thus, simulations match observed rates choosing $E_{\rm act}=E_c=0.75$ eV, an estimate that is more robust than that of J (which depends on the choice of E_e). In one test of this result for $E_{\rm act}$ we simultaneously adjusted E_e and J to maintain a constant E_c, and found negligible variation in the decay of the height of a 20×20 atom protrusion for E_e between 0.18 and 0.26 eV (but decay was slower for E_e above about 0.3 eV, corresponding to J below about 0.2 eV). Finally, we assessed the dependence of the decay rate for protrusions on J, as this corresponds to the fitting procedure used above. The results, presented in Table I, are consistent with $E_{\rm act}({\rm PD})\approx E_e+2J$.

One consequence of the simplification in our model excluding hopping of triply bonded atoms is that perfect [110] step edges are inactive or ''frozen.'' This could conceivably influence the decay of protrusions at these step edges, as could the finite system size of the simulations. (Our simulations use a finite length of step edge of at least five times the initial linear dimension of the protrusion, and apply periodic boundary conditions.) We have performed various tests, which indicate the robustness of our simulation results (including varying the system size, adding various fractions of a single layer of atoms to the initial step edge).

Experimental observations suggest that the decay of a square protrusion does not significantly perturb a perfectly aligned equilibrium [110] step edge. (This feature is enforced in simulations where perfect [110] step edges are inactive.) However, we emphasize that there can be a significant interplay between active atoms at the periphery of the protrusion, and active atoms on the step edge (either those which have flowed down from the protrusion, or those at kinks, etc., on an imperfect [110] step edge). A more detailed analysis of this interplay, and its consequences for the kinetics of the decay of protrusions, will be presented elsewhere.[47] Here, we just illustrate this point with an observation of direct experimental relevance. Invariably, in experiment, steps are at least slightly misaligned from the [110] direction. Then, one observes rapid adjustment of the step edge in the vicinity of the protrusion to achieve the [110] orientation. See Fig. 5. Specifically, mass supplied by nearby kinks accumulates on the uphill side of the protrusion, and mass is removed from the downhill side, creating [110] plateaus. Entirely analogous behavior is observed in simulations where a square cluster collides with a slightly misaligned [110] step edge. Figure 10 shows a corresponding sequence of simulated configurations.

TABLE I. Dependence on J (in eV) of the initial rate of decay of the height of protrusions at a [110] step edge at 298 K (for fixed $E_e=0.20$ eV). Values are shown in a/min for various sizes (in a^2 or atoms). Results come from averaging over at least 10 simulation runs for 0.275 eV, and at least 20 for 0.245 and 0.215 eV. They demonstrate that $E_{\rm act}({\rm PD})={\rm const}+2J$

J (in eV)	10×10	20×20	30×30
0.275	6.9	1.10	0.61
0.245	59.3	11.5	5.8
0.215	477	103	40

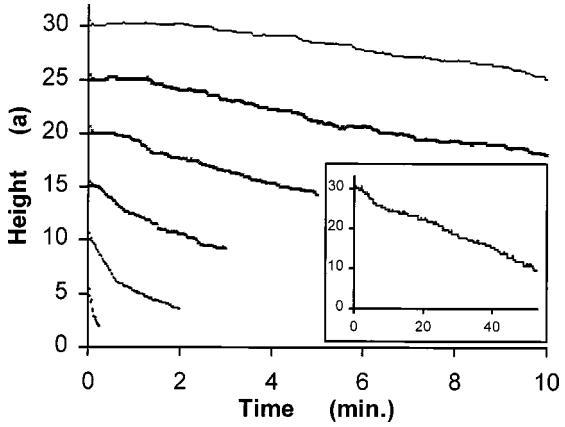

FIG. 9. PD model predictions for height versus time for the decay of initially square protrusions of linear dimension, $5a$, $10a$, $15a$, $20a$, $25a$, and $30a$ (from bottom to top) at a [110] step edge. These average over at least 10 simulation trials. The inset shows the decay of the height of a 30×30 atom protrusion over an extended period of time (averaged over two simulation trials), so the final height is only 30% of the initial height.

B. Cluster+[100] step coalescence

Figure 11 shows evolution after contact of the corner of a near-square roughly 50×50 atom cluster with a [100] step taken from Ref. 17. STM images reveal the *rapid* formation of a connecting meniscuslike neck. Simultaneously, one observes the creation of ''large'' indentations into the metastable [100] step edge, the sides of which have the preferred equilibrium [110] and $[1\bar{1}0]$ orientations. This behavior is apparent in the first five STM images in the sequence shown in Fig. 11. During this relaxation process, an intermediate stage is reached, where the step geometry consists of a near perfect right-angle triangle protruding from [100] step, the sides of this triangle selecting the preferred [110] and $[1\bar{1}0]$ orientations. See the sixth STM image in Fig. 11. Thereafter, one observes a slow decay of this triangular protrusion.

Various stages of the decay are quantified to some extent in Fig. 12(a). Here, we show the variation with time of maxi-

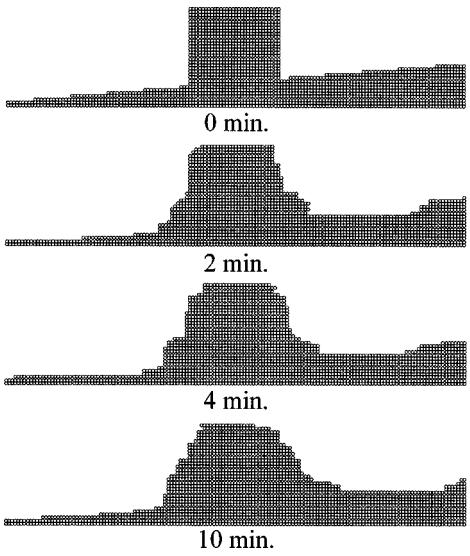

FIG. 10. Simulated sequence of configurations for restructuring following collision of a roughly square cluster having a linear dimension of about $30a$ with a slightly misaligned [110] step edge (cf. Fig. 5). The system size is $180a$ horizontally, of which a $151a$ stretch is shown in all snapshots. Skewed periodic boundary conditions are applied with a vertical offset of $15a$.

mum height $h_{\triangle}$ of the protrusion or nodule in Fig. 11, where $h_{\triangle}$ is measured relative to (and orthogonal to) the mean position of the step edge. The slow initial decrease of $h_{\triangle}$ is associated with growth of the still thin neck where mass flow to the step edge is inhibited. After a thick neck is formed, $h_{\triangle}$ decays quickly until a triangular configuration is reached. At that point (indicated by the arrow), there is a distinct decrease in the rate of decay. Similar behavior is observed for a smaller roughly 30×30 atom cluster, as shown in Fig. 12(b). Simulations of the decay process for this smaller 30×30 atom cluster size using our PD model at 298 K (with parameters as in Sec. IV A) are shown in Fig. 13, and reveal the same features as in experiment. The decay of height versus time, shown in Fig. 12(c) is similar to experimentally observed behavior in Fig. 12(b) for a cluster of roughly the same size (but see further comments below). Next, we analyze separately, and in more detail, both behavior in the initial regime of rapid neck growth, and in the later stage regime of decay of the triangular protrusion. All simulations are performed at 298 K with the same parameters as in Sec. IV A.

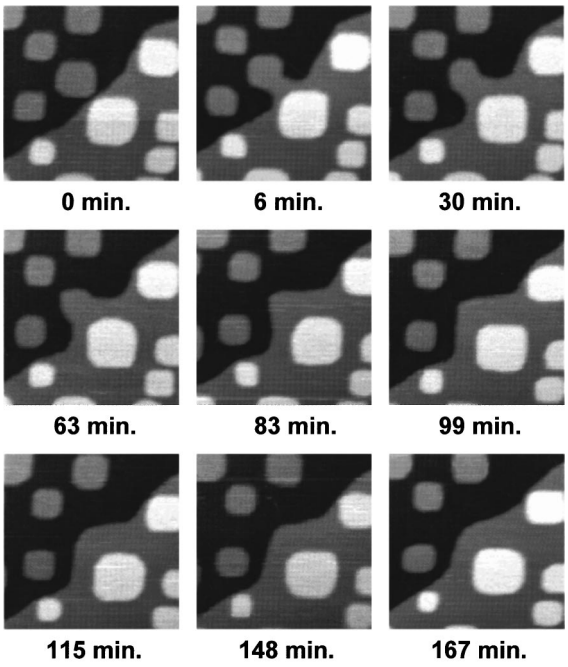

FIG. 11. Sequence of STM images from Ref. 17 showing coalescence of a 150×140 Å^2 cluster with a [100] step edge, and subsequent decay of the protrusion thus formed. All images are 725×725 Å^2.

First, we consider the *initial neck growth*. The above observation (both in experiment and simulation) of simultaneous neck growth and formation of indentations in the step edge indicates that this neck growth is primarily due to mass flow from the indentations to the neck, rather than from the cluster to the neck. In fact, due to this nearby large reservoir of mass in the step edge, initial neck growth occurs so rapidly that it is difficult to quantify precisely in experiment, at least for smaller cluster sizes. However, simulations can readily provide a more complete and precise picture, and also confirm the above claim regarding mass flow. Simulation results shown in Fig. 14 for the evolution of the width of the neck with time reveal a dramatic initial increase for about 1 min, followed by more sustained quasilinear growth. Note that the initial increase becomes independent of cluster size for large enough clusters, as growth is predominantly involves mass flow from the step edge to the neck. For a 50×50 atom cluster, simulations with the above parameters yield a rate of quasilinear growth at rate $G\approx3.1\,a/\,\mathrm{min}$, and produce a neck width of $35a\approx100$ Å after about 5 min. These results are entirely consistent with the experimental behavior for the case shown in Fig. 11.

Second, we consider the late-stage regime involving the *decay of the triangular protrusion* formed part way through the relaxation process. In Fig. 11, this corresponds to decay subsequent to the right-angled triangle configuration shown in the sixth image. The experimental decay rate of the triangle height at onset of this final stage $R_{\triangle}=dh_{\triangle}/dt$ is shown in Fig. 15 for various areas, A (which are actually taken from the cluster size prior to coalescence). We note that there are large fluctuations in this decay process, due in part to wandering and splitting of the protrusion peak, and that these produce substantial uncertainties in experimental values for $R_{\triangle}$. We compare this behavior against simulation predictions using our PD model with the above parameters. Since simulations starting with the configuration in Fig. 13 are so time consuming, we instead start with a perfect right-angled triangle attached to a perfect [110] step edge, and follow the decay of the height from that configuration. Results from these simulations for the initial decay rate $R_{\triangle}$ are also shown in Fig. 15, and are consistent with experiment (given the substantial uncertainties). These $R_{\triangle}$ values are substantially smaller than $R_{\square}$ values for similarly sized protrusions at the [110] step edge. Our simulations also suggest that again $E_{\mathrm{act}}=E_e+2J=E_c$. The comparison between $R_{\triangle}$ and $R_{\square}$, and the form of E_{act} are discussed in more detail in Sec. II C.

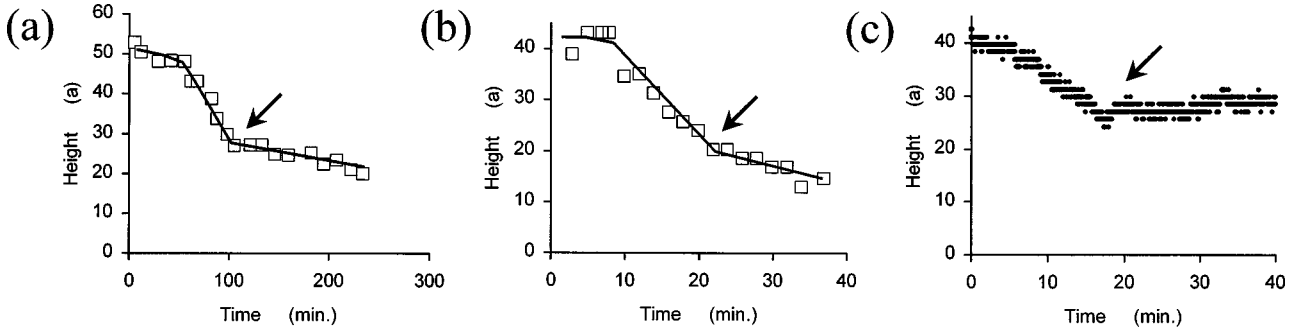

FIG. 12. Decay of height, measured orthogonal to the [100] step edge, of the protrusion produced by corner-on collision of (a) a roughly 50×50 atom cluster shown in Fig. 11, (b) a roughly 990 atom cluster (experiment).and, (c) a 30×30 atom cluster (a single simulation). The arrows indicate the time when a roughly triangular protrusion is formed at the [100] step edge, and the solid curves in (a) and (b) are only to guide the eye.

Finally, we mention one feature of our PD model, which requires attention when comparing against experimental observations. A perfect [100] step edge eventually facets into alternating portions of [110] and $[1\bar{1}0]$ orientations, since the latter are energetically preferred. The same process occurs with a protusion at a [100] step edge, where the faceting affects (and specifically slows down) the decay of protrusions for longer times. This is evident in the second stage of the decay shown in Fig. 12(c). However, this study has focused on the initial relaxation behavior, where typically faceting has not had sufficient time to develop or to affect measured behavior. The inhibition or lack of faceting of [100] step edges in the experiment can be due to a number of factors not included in the model. These include pinning of the step edge by higher layer islands or by impurities, or deviations from NN interactions in the Ag/Ag(100) system (which can reduce the ratio of the formation energies for [100] and [110] step edges[37] to a value below $\sqrt{2}$ associated with NN interactions, but still above unity).

C. Analysis and comparsion of behavior for [110] and [100] step edges

The key quantity controlling the overall decay rate, and particularly its temperature dependence, is the effective activation barrier $E_{\rm act}$(PD). Thus, further elucidation of this quantity is appropriate here. First consider the decay of a roughly square (or rectangular) protrusion on a [110] step edge, as shown schematically in Fig. 16(a). We note that at various stages of decay, it is necessary to disrupt the ''rectangular core'' of the protrusion, and that this requires ''core breakup.'' The same requirement was noted previously for diffusion of large 2D clusters.[27,29] This feature alone indicates that overall decay is limited by core breakup, suggesting that $E_{\rm act}({\rm PD})\approx E_c$. However, in addition to these slow core breakup steps, most of the height reduction process involves repeated kink escape *followed by* corner rounding [see Fig. 16(a)]. If $\rho_{eq}\approx h_k/h_e$ is the quasiequilibrium density of atoms released from the kink site (as in Sec. II B), then this *combined* process occurs at an effective rate[18]

$$h_{\rm cf}\sim\rho_{\rm eq}h_r\sim\nu\exp[-(E_e+2J)/(k_BT)]. \tag{9}$$

Another perspective on this combined process follows from writing the effective rate as $h_{\rm eff}\sim P_r h_k$. Here, P_r is the probability that an atom released from the top kink site (at rate h_k) successfully rounds the corner, rather than returning to the kink site. One can show that $P_r\sim h_r/h_e$, roughly independent of protrusion dimensions, so again one recovers the result (9) for $h_{\rm eff}$. Further details will be presented elsewhere.[47] Thus, both core breakup, and the combined height reduction process imply the same activation barrier, $E_{\rm act}({\rm PD})\approx E_e+2J(=E_c)$, consistent with simulation results. Second, we consider the decay of a roughly triangular protrusion on a [100] step edge shown schematically in Fig. 16(b). For this geometry, it is clear that a significant fraction of the mass transport during decay is mediated by core breakup steps, so again one has $E_{\rm act}({\rm PD})\approx E_e+2J(=E_c)$.

Next, we compare the experimental rates for decay of the height of square protrusions at [110] step edges (Fig. 7) with the rates for triangular protrusions at [100] step edges (Fig. 15), and derive some basic insights regarding the underlying mass-transport processes. The data reveal significantly larger rates for decay of protrusions on [110] step edges, compared with [100] step edges (for the same protrusion size). For example, $R_\square=0.42a/{\rm min.}$ $(1.1a/{\rm min.})$, when $A=1600a^2$ $(500a^2)$ for the former, versus $R_\triangle=0.05a/{\rm min.}$ $(0.46a/{\rm min.})$, when $A=2500a^2(650a^2)$ for the latter. In fact, these STM observations provide immediate insight into the dominant mass transport mechanism at step edges. They indicate a significant dependence of the efficiency of mass transport on step orientation. This, in turn, provides evidence for PD-dominated mass transport, since TD- or EC-dominated mass transport should have comparable efficiency for different orientations. The difference in efficiency of mass transport is readily understood within the context of our model: transport along [100] steps requires repeated slow core breakup steps, rather than easier kink escape steps (and very fast edge diffusion) which is sufficient for [110] steps.

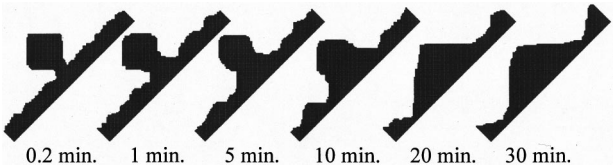

FIG. 13. Simulated sequence of configurations for a 30×30 atom cluster coalescing with a [100] step edge (of length $\sqrt{2}\times1000a$), and subsequent protrusion decay for up to 30 min of physical time. The portion of the [100] step edge shown in all snapshots has a length $\sqrt{2}\times101a$.

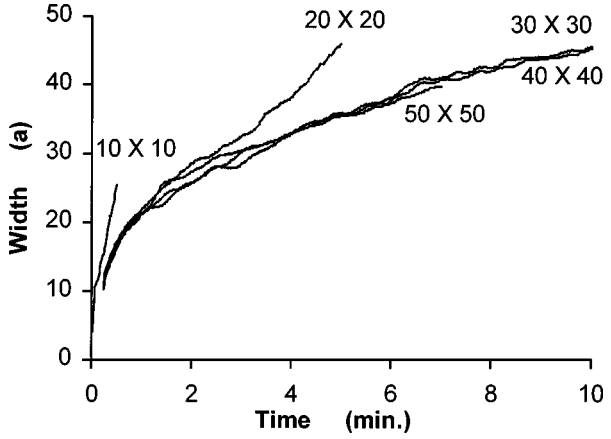

FIG. 14. Simulation predictions (averaging over 10 trials) for the growth of the ''neck width'' subsequent to coalescence with a [100] step edge of square clusters with side lengths of $10a$, $20a$, $30a$, $40a$, and $50a$.

These features are indicated in the schematics of Figs. 16(a) and 16(b). The situation in the real Ag/Ag(100) system may be different: it is possible that the barrier, $E_e[100]$, for diffusion of an atom along a perfect [100] step edge is substantially below E_c (see Sec. VIII). If $E_e[100] \approx E_k$, then the enhanced efficiency for [110] steps is less clear. For each difficult kink escape step, the atom potentially can travel a substantial distance to the next kink site, rather than just one or two hops as on a [100] step edge, but the density of mobile atoms is higher for the latter.

Our claim of PD-dominated mass transport is supported by several observations: (i) the step orientation dependence of the rate of decay of protrusions; (ii) our demonstration of an energetic advantage of PD over TD or EC; (iii) the consistency of our analysis of experimental data with a PD model for very different geometries and sizes (including coalescence of cluster pairs,[18] which is not discussed here); and (iv) by an experimental study suggesting that PD dominates mass transport associated with the diffusion of 2D Ag clusters on Ag(100). (This interpretation was questioned in Ref. 43, but see our comments in Sec. III B.) We emphasize, however, that at least TD mechanisms of mass transport always operate to some degree, in addition to PD. Furthermore, they could dominate PD under different conditions, e.g., higher T,

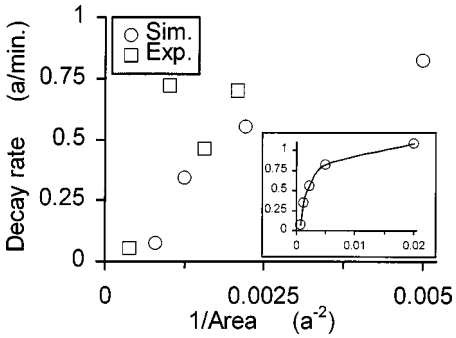

FIG. 15. Initial rate of decay of the height of a triangular protrusion at a [100] step edge versus 1/Area: ''squares'' represent experimental data, and ''circles'' represent PD model predictions with $J = 0.275$ eV. The inset shows nonlinear variation of rate with 1/Area in the PD model for a range of smaller protrusion sizes.

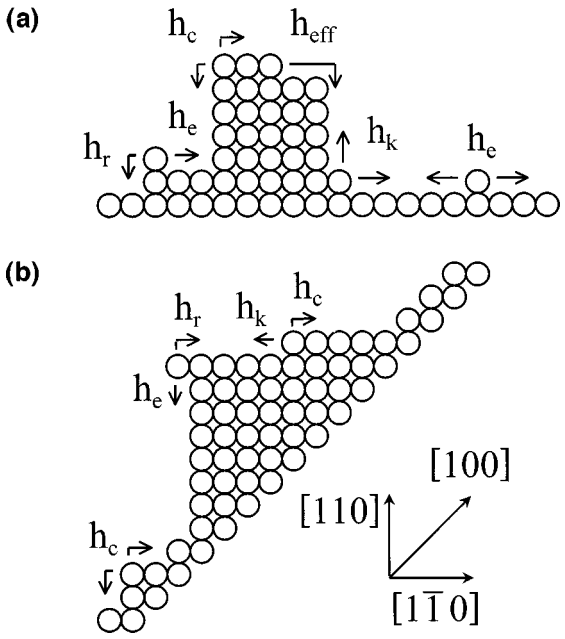

FIG. 16. Schematic showing (a) typical atomic hops, and their corresponding rates, producing decay of a near-square protrusion at a [110] step edge; h_{eff} represents the effective rate for an atom to escape a kink site and successfully round the corner; (b) typical atomic hops producing decay of a near-triangular protrusion at a [100] step edge.

or larger characteristic lengths of structures. Indeed, a few of our observations of the relaxation of the shapes of very large clusters, close to other clusters and to step edges, show evidence for pinned nonequilibrium shapes, indicating the presence of some EC processes (cf. Sec. III B).

V. VACANCY INDENTATIONS AT EXTENDED STEP EDGES

In this section, we briefly describe a study of the relaxation of vacancy indentations at extended step edges. These indentations are almost perfect ''mirror-images'' of the square and triangular protrusions at step edges discussed in Sec. IV. First, we discuss experimental observations and simulation results, and then provide some analysis of this behavior.

A. Experimental and simulation results

As noted in Sec. I, nanoindentations are typically formed after deposition of larger submonolayer amounts of Ag. As existing step edges advance across terraces, they incorporate

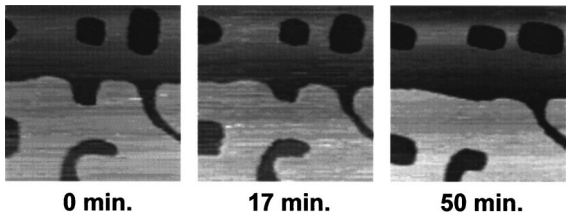

FIG. 17. Relaxation of a roughly 108×108 Å^2 vacancy indentation formed in an advancing [110] step edge during deposition of about 0.9 ML of Ag. All images are 730×730 Å^2.

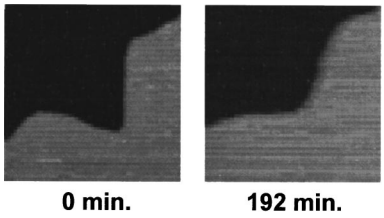

FIG. 18. Relaxation of a triangular vacancy indentation in a [100] step edge. Both images are 500×500 Å^2.

2D Ag clusters ahead of the step edge, resulting in a highly irregular step-edge structure. Rapid restructuring after terminating deposition often leaves locally straight steps with a few larger nanoindentations. Figure 17 presents a sequence of STM images illustrating the relaxation of a nearly square indentation with an area of about $1450a^2$, which was formed in a step edge with [110]-type orientation. The depth of the indentation is about $38a$ initially, and decays at a rate of about $0.7a$/min. The relaxation of a triangular indentation with an area of about $4000a^2$, formed in a step with [100]-type orientation, is shown in Fig. 18. Its depth is about $56a$ initially, and it decays at a rate of about $0.07a$/min. Assuming that decay rates scale roughly linearly with inverse area, the above examples suggest substantially higher decay rates for square indentations at [110] steps than for triangular indentations of the same size at [100] steps. Analysis of the rather limited data for the decay of the depth of indentations at [110] step edges suggests comparable or perhaps somewhat higher decay rates than for adatom protrusions of the same size.

We have performed simulations of the decay of indentations using exactly the same periphery diffusion model described in Sec. III A, and applied in analyzing the decay of protrusions in Sec. IV. Figure 19 shows a sequence of configurations during the decay of a square indentation at a

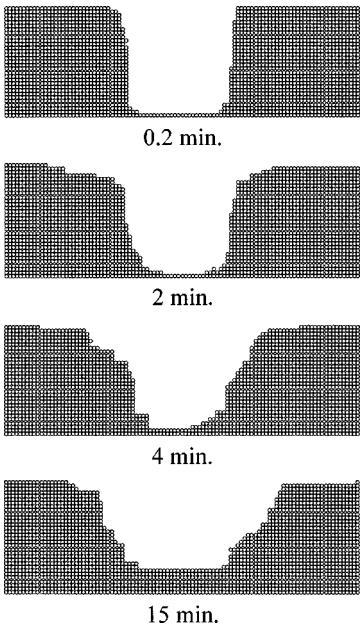

FIG. 19. Simulated sequence of configurations for a $30a\times30a$ vacancy indentation decaying on a [110] step edge (of length $180a$).

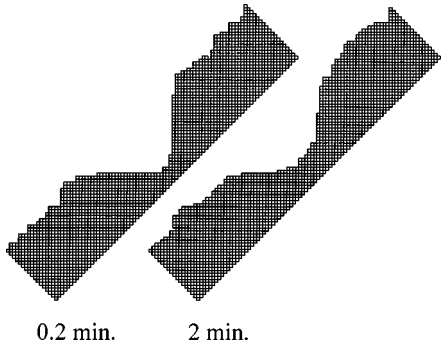

FIG. 20. Two snapshots decaying vacancy indentation at a [100] step edge with an initially $\frac{1}{2}\times30\times30$ triangular shape. The length of the [100] step edge is $\sqrt{2}\times180a$, from which only a portion of length $\sqrt{2}\times81a$ is shown.

[110] step edge, and Fig. 20 shows the decay of a triangular indentation at a [100] step edge. We emphasize that this PD model does *not* treat adatoms and vacancies in an equivalent way, so the decay process for a square indentation will be quite different from that for a square protrusion. Specifically, adatoms first ''peel off'' the top of a protrusion away from the step edge, whereas atoms at the base adjacent to the step edge are inactive (being triply bonded). In contrast, atoms at the ''entrance'' of an indentation next to the step edge are active and can flow into the indentation, whereas those at the bottom of the indentation furthest away from the step edge are inactive (being triply bonded.) A more detailed discussion of this issue, and of alternative models, is given below in Sec. V B. Here, in Table II, we just compare predictions for this model for initial rates of decay for the depth of the indentations at 298 K with corresponding decay rates for protrusion height. The same choice of parameters is used as previously. Interestingly, the decay rates for protrusions and indentations are quite similar, despite the difference in the underlying mass transport process. The value predicted for the decay rate of a protrusion of the size shown in Fig. 17 (of about $0.4a$/ min) appears somewhat smaller than the experimental observation ($0.7a$/ min), but the difference is within the experimental uncertainty.

B. Adatom-advacancy inequivalence

For an adlayer described by NN interactions, the equilibrium properties of adatom cluster configurations (at x ML, say) and vacancy cluster configurations (at $1-x$ ML) are equivalent (particle-vacancy symmetry). However, this equivalence does *not* necessarily apply to nonequilibrium kinetics. In the latter case, behavior is controlled by activation barriers for hopping. Particle-vacancy asymmetry in these

TABLE II. Comparison of initial rates of decay for the height of protrusions and the depth of indentations at [110] step edges, at 298 K. Values are shown in a/min for various sizes (in a^2 or atoms). Results come from averaging over 10 simulation runs.

Size	10×10	15×15	20×20	25×25	30×30
Protrusions	6.9	1.9	1.1	0.92	0.61
Indentations	6.3	2.1	1.0	0.57	0.41

quantities was shown very clearly in semiempirical EAM studies by Voter for the Ag/Ag(100) system (although one does not have pure NN interactions in this system).[29] To provide an experimental example, we note that the diffusion coefficient D is a factor of two or three higher for large adatom clusters than for large vacancy clusters (of the same size) in the Ag/Ag(100) system.[20] Given the above observations, we emphasize that models which accurately describe *far-from-equilibrium* kinetics will not in general exhibit particle-vacancy symmetry. Indeed, our simple PD model does not have this symmetry. However, it was formulated to realistically describe the hopping processes mediating the decay of protrusions at step edges where local configurations are convex. It is not clear that it appropriately describes key hopping processes for indentations where local configurations are concave. For these reasons, some reassessment of our model, and consideration of alternatives, is appropriate.

In any model that treats adatoms and vacancies ''equivalently,'' one would need to allow additional edge hopping processes (including hopping of triply bonded atoms). In particular, such processes include the ''sliding process'' shown in Fig. 21(a), which is the direct analogue of the key core breakup process for adatoms shown in Fig. 16(a) (and Fig. 3). The rate for sliding is denoted by $h_s = \nu \exp[-E_s/(k_BT)]$. The original semiempirical studies by Voter[29] for Ag/Ag(100), and more recent generic categorizations of hopping barriers for metal(100) homoepitaxial systems,[33,34] both indicate that the activation barrier, E_s, is *less* than that for core breakup. An estimate of $E_s \approx E_e + 1.5J$ is not unreasonable. Thus, one has $E_s < E_c$ despite the fact that sliding nominally involves triple bond breaking. This feature is due to the presence of strong interactions in the transition state (cf. Sec. III A). Despite this inequality, removal of atoms further from the corner sites via the sliding mechanism actually occurs at a rate comparable to (not faster than) that for core breakup. This can be seen by the following argument. Once the atom has slid out of its initial position, suppose that subsequent hopping along the step edge occurs at rate h_e. Then, by detailed balance, the rate for the reverse process, $h_e' = \nu \exp[-E_e'/(k_BT)]$, must satisfy

$$h_e'/h_s = \exp[2J/(k_BT)],$$

$$\text{so } E_e' = E_s - 2J \approx E_e - 0.5J \text{ if } E_s \approx E_e + 1.5J. \quad (10)$$

Since $E_e' < E_e$, return is more likely than continued motion away from the corner, and the population, $\rho_s \sim h_s/h_e'$, of the configuration in Fig. 21(b) is very low. The effective rate for removal of atoms further from the corner site initiated via sliding equals $\rho_s h_e$, and the effective barrier for this pathway equals $E_e + 2J$, as for core breakup. Thus, sliding provides an alternative pathway at least for the initial restructuring of indentations, which is competitive with those included in our PD model. However, its ultimate effectiveness is not clear.[47] (If it is ineffective, our current asymmetric PD model may suffice to accurately describe the decay of indentations.)

VI. NANOFABRICATION OF RECTANGULAR PROTRUSIONS AT [110] STEP EDGES

The interaction of the STM tip with the surface can be utilized to fabricate far-from-equilibrium step-edge nanostructures more exotic than provided naturally by deposition, or by post-deposition evolution. To this end, one typically adjusts scanning conditions to amplify the influence of the tip, in contrast to the studies described above. For the Ag(100) system, we find that mass can be drawn out in a ''finger'' roughly perpendicular to a [110] step edge. If this finger merges with an island on the terrace, then the connected structure reshapes to ''automatically'' form a near-rectangular protrusion extending orthogonal to the step edge. This protrusion then shortens and thickens finally decaying into the largely unperturbed step. Figure 22 presents a sequence of STM images showing this formation and relaxation sequence. Of course, studies of the relaxation of such rectangular protrusions naturally extend the analysis in Sec. IVA for square protrusions.

Given the limited experimental data, we focus on a simulation analyses of the decay of rectangular protrusions orthogonal to [110] step edges at 298 K. We use our PD model with the same parameters as previously. Figure 23 shows a sequence of images for the decay of a 135×15atom protrusion. More generally, we have determined the initial rate of decay of the height for rectangular protrusions with a fixed width of 15 atoms (as in Fig. 23), and various initial heights between 15 and 135 atoms. This decay rate as a function of protrusion area is shown in Fig. 24. The rate first decreases as the initial height is increased to be larger than the width (increasing the area), analogous to behavior for square protrusions in Fig. 7. Then, for even larger initial heights (more elongated rectangles), the rate increases again, approaching a finite (nonzero) limiting value for infinite length. Certainly, a nonzero limiting value is expected since an infinitely long protrusion or rectangular islands is not stable, and should contract in length. The nonmonotonic variation of rate with length or area is less easy to anticipate. Some further discussion is provided in Sec. VII.

Less controlled creation (and subsequent relaxation) of irregular protrusions, as a result of the STM-tip drawing mass out from step edges on the Ag(110) surface, was noted previously in Ref. 13. No doubt this is a general phenomenon for metal surfaces. It would thus allow for the possibility in many systems of studying mass transport at step edges by first creating desired far-from-equilibrium configurations, and then monitoring their relaxation. One would not have to rely on, e.g., the diffusion of large clusters to step edges, in order for nanoprotrusions to be formed.

VII. COMPARISON WITH CONTINUUM THEORY

In a coarse-grained picture,[16,26] the location of the step edge is described by a continuous curve. Let ''s'' denote the distance along the curve, C the curvature, θ the local orien-

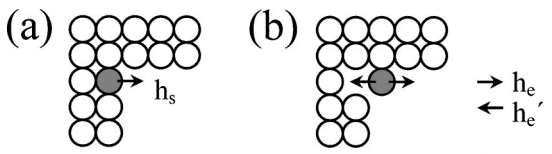

FIG. 21. Schematic showing: (a) ''sliding'' of an atom out from the corner of a vacancy indentation at rate h_s; (b) continued hopping of this atom along the [110] step edge at rate h_e, or return to the corner site at rate h_e'.

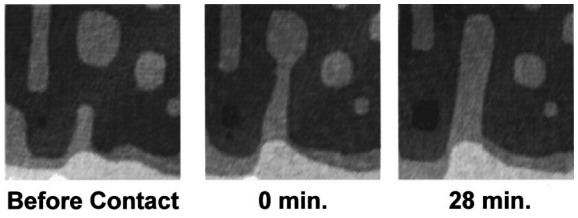

FIG. 22. Sequence of STM images showing the formation of a rectangular protrusion orthogonal to an undulating [110] step edge by drawing out a ''finger'' of atoms from the step edge to coalesce with a 2D island. All images are 770×770 Å^2.

tation, $\beta(\theta)$ the step-edge free energy, and $\mu(\theta)$ the step-edge chemical potential. Then, one has

$$\mu\propto\beta^*C, \quad \text{where} \quad \beta^*=\beta+\partial^2\beta/\partial^2\theta. \tag{11}$$

Evolution is driven by minimization of the step free energy, and the mass flux J *along* the curve satisfies $J\propto -d/ds\mu$. Consequently, mass continuity implies that the propagation velocity of the step edge normal to the step edge V satisfies

$$V_\perp=-d/dsJ\propto -d^2/ds^2[\beta^*C], \tag{12}$$

where $V_\perp>0$ means motion to the left of the direction corresponding to increasing s.

This equation can be used to analyze the decay of the height, $h(x)$, of protrusions or indentations at step edges oriented in the x direction. The simplest approximation neglects the orientation dependence of β [which is strong for Ag(100)], and assumes small slopes, so ''s'' is replaced by ''x.'' Then Eq. (12) reduces to the linear Mullins equation,[48]

$$\partial h/\partial t\propto -\partial^4 h/\partial x^4, \tag{13}$$

which can be readily analyzed by Fourier transformation. The key results are that that the characteristic decay time τ for a perturbation of the straight step edge of wavelength, q, scales like[16] $\tau\propto q,^4$ and that the maximum height of the protrusion or indentation, $h_{\max}$, decreases asymptotically to zero with time t like $h_{\max}\sim t^{-1/4}$.

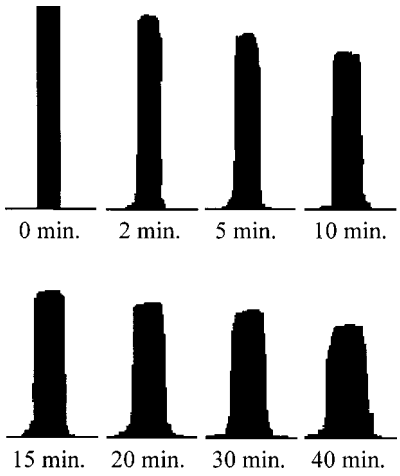

FIG. 23. Simulated sequence of configurations for an initially 135×15 atom rectangular protrusion decaying at a [110] step edge (of length $150a$), for up to 40 min of physical time. A fixed segment of step edge of $90a$ is shown.

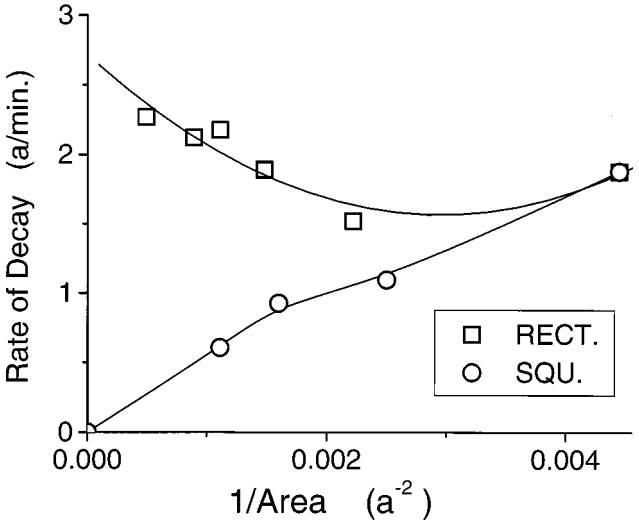

FIG. 24. Simulation predictions (averaging over 10 trials) for the initial rate of decay of the height of initially rectangular protrusions of fixed initial width of $15a$ and various heights $(15a,30a,45a,60a,75a,135a)$ at a [110] step edge versus 1/Area (square symbols). Included, for contrast, are decay rates for initially square protrusions (circular symbols).

These results are not so instructive for our study where we focus on ''initial'' decay rates, $R=V_\perp(t=0)$. Instead, it is more useful to consider protrusions or indentations with a specific shape, but varying size, so we write $h(x)=La(x/L)$. Here $a(y)\to0$, as $y\to\pm\infty$, is a shape function assumed to be *even*, with a maximum at $y=0$. Here, L is the linear size parameter, so the area scales like $A\propto L^2$. Then, neglecting the θ dependence of β, but exactly calculating the derivatives with respect to s (rather than using small gradient approximations), one obtains

$$R=V_\perp(x=0)\propto L^{-3}[a''''(0)-3\{a''(0)\}^3]. \tag{14}$$

Thus, the continuum theory predicts that $R\sim A^{-3/2}$, in contrast to the behavior $R\sim A^{-1}$ seen in simulation and experiment for the range of sizes of experimental relevance (see Fig. 7). One can also consider protrusions or indentations of fixed width, but varying height. Then, one has $h(x)=Lb(x)$, with shape function $b(x)$, and L is the linear height parameter. Neglecting the θ dependence of β, one finds that $V_\perp\propto L$, a direct consequence of the linearity of the Mullins equation.[48] This increase in the decay rate with height in part reflects the behavior observed in simulations for rectangular protrusions (see Fig. 24). Certainly, including anisotropy in step edge energetics would capture better basic geometric features, and modify decay dynamics. However, even then, it is likely that continuum treatments cannot precisely capture subtleties of kinetics on the small length scales of relevance in our studies.

VIII. DISCUSSION OF INTERACTION ENERGIES AND MODEL REFINEMENTS

In our PD model, the *effective* NN pairwise interaction strength J was identified as the key free parameter to be adjusted to fit experimental behavior. We thus obtained an estimate of $J=0.275$ eV (assuming that $E_e=0.20$ eV) for the

Ag/Ag(100) system. We note that using effective NN interactions to describe the transition to reversible island formation during deposition of Ag on Ag(100) yields a consistent estimate[35] of $J \approx 0.3$ eV. However, it has been suggested that such J values are far too high.[49] Thus, it is appropriate to mention that *ab-initio* generalized gradient approximation (GGA) calculations[37] for the detachment of an atom from a [110] step edge predict that $E_b = 0.76$ eV (compared with $E_d = 0.45$ eV), and that the energy change in the binding site is consistently given by 0.32 eV ($\approx E_b - E_d$). For NN interactions, this value of 0.32 eV would correspond to J. In fact, one expects that this value slightly overestimates J due to the presence of weak next NN interactions. Indeed, semiempirical studies suggest the relationship $J \approx 0.85(E_b - E_d)$ yielding a GGA-based estimate of $J = 0.27$ eV, entirely consistent with this study.

There has been a detailed experimental STM study of the equilibrium fluctuations at [110] step edges in the Ag/Ag(100) system.[50] A conventional analysis of this data produced an estimate for the ''kink creation energy'' of $E_{\rm kink} \approx 0.114$ eV. This is reasonably consistent with our results, noting that $E_{\rm kink} = J/2$ for NN pairwise interactions, and that the details of near-equilibrium fluctuations could be more sensitive to deviations from NN interactions.

It is also appropriate to note that the model developed here may well apply to describe similar behavior in other metal(100) systems. Analogous restructuring has been reported for Cu/Cu(100) at 295 K, but at substantially higher rates.[4,22] Assuming that PD dominates,[4,22] one concludes that $E_{\rm act}({\rm PD}) \approx E_e + 2J < 0.75$ eV for Cu/Cu(100). This inequality is consistent with a GGA estimate[47] of $J = 0.22$ eV, and an estimate of E_e given by $E_d/2$ using the best experimental value[51] of $E_d = 0.36$ eV. (However, one obtains $E_e + 2J > 0.75$ eV using the GGA estimate[46] of $E_d = 0.52$ eV.) These observations suggest that $J_{\rm Cu} < J_{\rm Ag}$, consistent with estimates from analyses of island formation process,[52] but contrasting expectations based on bulk cohesive energies.[49]

Although in our modeling, we treat interactions between adatoms in their adsorption sites as NN pairwise, this is an oversimplification. If one describes actual interactions within the framework of pairwise interactions, based on semiempirical studies, one would expect weak next-NN attractive interactions to be present with about 10% of the NN interaction strength.[29,34] More realistically, one would expect the presence of weak many-body interactions. Certainly, incorporating longer range or many-body interactions into the modeling would modify the estimate of J (which should be regarded as an effective NN interaction strength), but probably not dramatically.

It is likely that in order to describe precisely relaxation behavior beyond initial decay or restructuring rates, other modifications to the *kinetics* of our model may be appropriate. (These could be made still within the framework of NN interactions.) Here, we mention two possibilities, the influence of will be considered in detail in a separate paper.[47]

(i) It is well recognized that concerted or exchange atom motions, rather than just single particle hopping, can be important in diffusion, growth, and relaxation processes. One possibility of particular relevance here is ''concerted corner rounding'' where an isolated atom running along a straight [110] edge exchanges with a corner atom, thus effectively rounding the corner. At least for corners corresponding to single-atom high kinks, it seems quite plausible that this process could have a lower barrier than the barrier E_r for conventional corner rounding shown in Fig. 3. Such an ''easy corner rounding pathway'' would lead to an *increase* in the effective rate for corner rounding, $h_{\rm eff}$, which was described in Sec. IV C. Even if just restricted to single atom high kinks, it should at least enhance the later stage decay of square protrusions at [110] step edges. It seems less likely that this concerted process should be significantly more favorable than conventional corner rounding at corners corresponding to multiple atom high kinks.

(ii) Another possible modification to the model is to allow the activation barrier $E_e[100]$ for hopping of an atom along a perfect [100] step edge (''stair climbing'') to be distinct from that for core breakup E_c. If $E_e[100] < E_c$, then this could enhance the rate of decay of triangular protrusions at [100] step edges (relative to our PD model). Some motivation for this selection is provided by semiempirical studies for Ag/Ag(100).[53] These find that $E_e[100] \approx 0.46$ eV, whereas $E_e \approx 0.26$ eV and $J \approx 0.28$ eV, so $E_c \approx 0.82$ eV is in fact much larger $E_e[100]$. However, more recent EAM calculations suggest that $E_e[100] \approx E_c$.[54]

IV. CONCLUSIONS

We have characterized the decay of far-from-equilibrium step-edge nanostructures in the Ag/Ag(100) system. These structures form as a result of the post-deposition diffusion and subsequent collision with step edges of large 2D adatom clusters, and as a result of the advance of step edges during deposition. A simple lattice-gas model for periphery diffusion (PD) provides a remarkably consistent description of the decay rates for various local geometries (cf. Ref. 18), and also reproduces key features of the evolving nanostructure morphology. Matching initial decay rates provides an estimate of the key activation barrier, $E_{\rm ac}({\rm PD})$ for the overall PD process, which for our model corresponds to the barrier for ''core breakup'' of $E_c = E_e + 2J \approx 0.75$ eV. This quantity is not effectively probed by near-equilibrium studies. The prevalence of PD in this system is related to its energetic advantage over TD or EC which is in turn related to the fact that E_e is significantly less than E_d (see Ref. 55) or E_v. We also propose that extensive opportunities for studying the restructuring of a variety of exotic step edge nanostructures in this and other systems are provided by the possibility of using the STM tip to fabricate such structures. Finally, it is appropriate to note that the current intense interest in fabrication of far-from-equilibrium nanostructures in surface systems[56] fosters a need for studies such as this one which can elucidate mechanisms and rates for decay of such structures.

ACKNOWLEDGMENTS

This work was supported by NSF Grant No. CHE-9700592, and performed at Ames Laboratory, which is operated for the U.S. DOE by Iowa State University under Contract No. W-7405-Eng-82.

[1] L. Onsager, Phys. Rev. **37**, 405 (1931); **38**, 2265 (1931).
[2] H.-J. Ernst, F. Fabre, and J. Lapujoulade, Phys. Rev. Lett. **69**, 458 (1992).
[3] J.-M. Wen, J. W. Evans, M. C. Bartelt, J. W. Burnett, and P. A. Thiel, Phys. Rev. Lett. **76**, 652 (1996).
[4] W. W. Pai, A. K. Swan, Z. Zhang, and J. F. Wendelken, Phys. Rev. Lett. **79**, 3210 (1997).
[5] K. Morgenstern, G. Rosenfeld, and G. Comsa, Phys. Rev. Lett. **76**, 2113 (1996); J. B. Hannon, C. Klunker, M. Giesen, H. Ibach, N. C. Bartelt, and J. C. Hamilton, *ibid.*, **79**, 2506 (1997); G. S. Icking-Konert, M. Giesen, and H. Ibach, Surf. Sci. **398**, 37 (1998).
[6] B. H. Cooper, D. R. Peale, J. G. McLean, R. Phillips, and E. Chason, in *Evolution of Surface and Thin Film Microstructure*, edited by H. A. Atwater, E. Chason, M. Graber, and M. Lagally, MRS Symposia Proceedings No. 280 (Materials Research Society, Pittsburgh, 1993), p. 37.
[7] J.-K. Zuo and J. F. Wendelken, Phys. Rev. Lett. **70**, 1662 (1993).
[8] M. Giesen, G. S. Icking-Konert, and H. Ibach, Phys. Rev. Lett. **80**, 552 (1998).
[9] K. Morgenstern, G. Rosenfeld, E. Laegsgaard, F. Besenbacher, and G. Comsa, Phys. Rev. Lett. **80**, 556 (1998).
[10] Z. Zhang and M. G. Lagally, *Morphological Organization in Epitaxial Growth and Removal* (World Scientific, Singapore, 1998).
[11] L. Kuipers, M. S. Hoogeman, and J. W. M. Frenken, Phys. Rev. Lett. **71**, 3517 (1993); M. Giesen-Siebert, R. Jentjens, M. Poensgen, and H. Ibach, *ibid.* **71**, 3521 (1993).
[12] R. C. Jakevic and L. Elie, Phys. Rev. Lett. **60**, 120 (1988); see also F. Mugle, A. Rettenberger, J. Boneberg, and P. Leiderer, Surf. Sci. **400**, 80 (1998).
[13] J. Li, R. Berndt, and W.-D. Schneider, Phys. Rev. Lett. **76**, 1888 (1996).
[14] B. S. Swartzentruber, Y.-W. Mo, R. Kariotis, M. G. Lagally, and M. B. Webb, Phys. Rev. Lett. **65**, 1913 (1990).
[15] E. J. Heller, Z. Y. Zhang, and M. G. Lagally, Phys. Rev. Lett. **71**, 743 (1993); F. Wu, X. Chen, Z. Zhang, and M. G. Lagally, *ibid.* **74**, 574 (1995).
[16] E. D. Williams, Surf. Sci. **299/300**, 502 (1994).
[17] J.-M. Wen, Ph.D. thesis, Iowa State University, 1995.
[18] C. R. Stoldt, A. M. Cadilhe, C. J. Jenks, J.-M. Wen, J. W. Evans, and P. A. Thiel, Phys. Rev. Lett. **81**, 2950 (1998).
[19] C. R. Stoldt, A. M. Cadilhe, M. C. Bartelt, C. J. Jenks, P. A. Thiel, and J. W. Evans, Prog. Surf. Sci. **59**, 67 (1998).
[20] P. A. Thiel and J. W. Evans, *Morphological Organization in Epitaxial Growth and Removal* (Ref. 10), p. 384.
[21] M. Giesen and G. S. Icking-Konert, Surf. Sci. **412/413**, 645 (1998).
[22] J. F. Wendelken, A. K. Swan, W.-W. Pai, and J.-K. Zuo, *Morphological Organization in Epitaxial Growth and Removal* (Ref. 10), p. 320.
[23] M. Esser, K. Morgenstern, G. Rosenfeld, and G. Comsa, Surf. Sci. **402–404**, 341 (1998).
[24] R. Kern, G. Le Lay, and J. J. Metois, in *Current Topics in Materials Science*, edited by E. Kaldis (North-Holland, Amsterdam, 1979), Vol. 3, Ch. 3.
[25] J. Eggers, Phys. Rev. Lett. **80**, 2634 (1998).
[26] S. V. Khare and T. L. Einstein, Phys. Rev. B **57**, 4782 (1998); **54**, 11 752 (1996).
[27] J.-M. Wen, S.-L. Chang, J. W. Burnett, J. W. Evans, and P. A. Thiel, Phys. Rev. Lett. **73**, 2591 (1994).
[28] A. Pimpinelli, J. Villain, D. E. Wolf, J. J. Metois, J. C. Heyraud, I. Elkinani, and G. Uimin, Surf. Sci. **295**, 143 (1993).
[29] A. F. Voter, Proc. SPIE **821**, 214 (1987).
[30] H. C. Kang, P. A. Thiel, and J. W. Evans, J. Chem. Phys. **93**, 9018 (1990); J. Soler, Phys. Rev. B **50**, 5578 (1994); **53**, R10 540 (1996); S. V. Khare, N. C. Bartelt, and T. L. Einstein, Phys. Rev. Lett. **75**, 2148 (1995); D. S. Sholl and R. T. Skodje, *ibid.* **75**, 3158 (1995); A. Bogicevic, S. Liu, J. Jacobsen, B. Lundqvist, and H. Metiu, Phys. Rev. B **57**, R9459 (1998); J. R. Sanchez and J. W. Evans, *ibid.* **59**, 3224 (1999).
[31] M. C. Bartelt and J. W. Evans, Surf. Sci. **314**, L829 (1994); Z. Y. Zhang, X. Chen, and M. G. Lagally, Phys. Rev. Lett. **73**, 1829 (1994); J. W. Evans and M. C. Bartelt, *Morphological Organization in Epitaxial Growth and Removal* (Ref. 10), p. 50.
[32] H. Shao, S. Liu, and H. Metiu, Phys. Rev. B **51**, 7827 (1995).
[33] M. Langelaar, Ph.D. thesis, Groningen University, 1998.
[34] O. Biham, I. Furman, M. Karimi, G. Vidali, R. Kennett, and H. Zeng, Surf. Sci. **400**, 29 (1998); M. Breeman, G. T. Barkema, and D. O. Boerma, *ibid.* **303**, 25 (1993).
[35] C.-M. Zhang, M. C. Bartelt, J.-M. Wen, C. J. Jenks, J. W. Evans, and P. A. Thiel, Surf. Sci. **406**, 178 (1998); L. Bardotti, C. R. Stoldt, C. J. Jenks, M. C. Bartelt, J. W. Evans, and P. A. Thiel, Phys. Rev. B **57**, 12 544 (1998).
[36] M. Langelaar, M. Breeman, and D. O. Boerma, Surf. Sci. **352/354**, 597 (1996).
[37] B. D. Yu and M. Scheffler, Phys. Rev. Lett. **77**, 1095 (1996); Phys. Rev. B **55**, 13 916 (1997).
[38] The study in Ref. 34 suggests the relation $E_e \approx E_d - J$, which is distinct from our assignment of $E_e = E_d/2$. [The two choices agree if $E_d \approx 2J$, which may be roughly satisfied in metal(100) homoepitaxial systems.] However, for Ag/Ag(100), our assignment is certainly reasonable.
[39] S. Clarke and D. D. Vvedensky, J. Appl. Phys. **63**, 2272 (1988).
[40] A. F. Voter, Phys. Rev. B **34**, 6819 (1986).
[41] H. Shao, P. C. Weaklim, and H. Metiu, Phys. Rev. B **53**, 16 041 (1996).
[42] D. P. Woodruff, G.-C. Wang, and T.-M. Lu, in *The Chemical Physics of Solid Surfaces and Heterogeneous Catalysis*, edited by D. A. King and D. P. Woodruff (Elsevier, Amsterdam, 1983), Vol. 2, Chap. 4.
[43] J. Heinonen, I. Koponen, J. Merikoski, and T. Ala-Nissila, Phys. Rev. Lett. **82**, 2733 (1999).
[44] P. Stoltze, J. Phys.: Condens. Matter **6**, 9495 (1994).
[45] EMT calculations in Ref. 44 indicate that $E_e = 0.25$ eV, $E_d = 0.49$ eV, and $E_v = 0.42$ eV for Ag/Ag(100), and $E_e = 0.25$ eV, $E_d = 0.43$ eV, and $E_v = 0.44$ eV for Cu/Cu(100). GGA studies in Ref. 46 indicate that $E_v/E_d = 0.8$ for Cu/Cu(100).
[46] G. Boisvert and L. J. Lewis, Phys. Rev. B **56**, 7643 (1997).
[47] A. M. Cadilhe and J. W. Evans (unpublished).
[48] W. W. Mullins, J. Appl. Phys. **30**, 77 (1959).
[49] P. J. Feibelman, Phys. Rev. B **52**, 12 444 (1995); (unpublished).
[50] M. S. Hoogeman, D. C. Schloesser, J. B. Sanders, L. Kuipers, and J. W. M. Frenken, Phys. Rev. B **53**, R13 299 (1996).
[51] H. Durr, J. F. Wendelken, and J.-K. Zuo, Surf. Sci. **328**, L527 (1995).
[52] J. W. Evans and M. C. Bartelt, in *Surface Diffusion: Atomistic and Collective Processes*, edited by M. C. Tringides (Plenum, New York, 1997), p. 197; M. C. Bartelt, L. S. Perkins, and J. W. Evans, Surf. Sci. **344**, L1193 (1995).

[53] R. C. Nelson, T. L. Einstein, S. V. Khare, and P. J. Rous, Surf. Sci. **295**, 462 (1993).
[54] U. Kürpick and T. S. Rahman, Phys. Rev. B **57**, 2482 (1998).
[55] This contrast typical behavior in metal(111) homoepitaxial systems (Ref. 10). The inequality $E_e < E_d$ ensures that $E_r < E_d + J$ (the latter constituting the effective barrier for dimer dissociation). Thus, corner rounding can occur when dimer dissociation is inactive, allowing the formation of compact islands during irreversible island formation in metal(100) homoepitaxy.
[56] J. A. Stroscio and D. Eigler, Science **29**, 1319 (1991).